Design and simulation of a vehicle-to-grid system

Simone Castellan
Dept. of Engineering & Architecture
University of Trieste
Trieste, Italy
scastellan@units.it

Nicola Blasuttigh
Dept. of Engineering & Architecture
University of Trieste
Trieste, Italy
nicola.blasuttigh@phd.units.it

Roberto Menis
Dept. of Engineering & Architecture
University of Trieste
Trieste, Italy
roberto.menis@dia.units.it

Alessandro Massi Pavan
Dept. of Engineering & Architecture
University of Trieste
Trieste, Italy
apavan@units.it

Mario Mezzarobba
Dept. of Engineering & Architecture
University of Trieste
Trieste, Italy
mmezzarobba@units.it

Giuseppe Buja
Dept. of Industrial Engineering
University of Padova
Padova, Italy
giuseppe.buja@unipd.it

***Abstract*—Batteries of electric vehicles have to be charged by power electronic converters connected to the electric grid. If these power converters are bidirectional they can be exploited to act in support to the grid operation, thus realizing the so called vehicle-to-grid (V2G) systems. At the University of Trieste an experimental V2G apparatus is under construction. Its control system has been developed and the first simulation tests has been performed. The paper describes the V2G experimental apparatus with its control system and reports the results of the preliminary simulation tests.**

Keywords— vehicle-to-grid, batteries of electric vehicles, three phase dual active bridge, ancillary services, smart grids.

I. Introduction

Battery-powered electric vehicles (EVs) and plug-in hybrid electric vehicles (PHEVs), commonly designated with plug-in EVs (PEVs), are entering more and more in the market because of the needs of reducing the fossil fuel consumption and of abating the environment pollution, especially in cities.

The use of the today's battery chargers that are able only to drawn power from the grid represents merely a load for the grid. On the contrary, if the PEV batteries were connected to the grid by means of bidirectional power apparatuses able not only to charge the batteries but also to exchange power with the grid, the PEV power capability could be exploited to execute services in support of the grid operations. Such services are commonly termed ancillary services and the expression vehicle-to-grid (V2G) has been coined to denote the services when due to the power transactions of the PEVs with the grid [1]-[4]. Typical ancillary services are voltage and frequency regulations, filtering of line harmonics, balancing of unbalanced loads, compensation of reactive power, spinning reserve and peak shaving.

Under this perspective, the V2G power transactions are expected to play an important role in the future scenario of the electric energy systems. The V2G apparatuses are able to carry out ancillary services which can involve either a net flow of active power with the grid or not [5]. In the first case the V2G services can be directed to support the grid by acting the PEV batteries as an energy buffer. In the second case, the V2G services can be directed both to stabilize the grid voltage and to improve the power quality.

An effective exploitation of the V2G apparatuses is undoubtedly obtained when they are connected to a smart grid [6]-[9]; this means that the control systems of the V2G apparatuses are networked with the grid administrator via communication devices to send it data on the operability of the apparatuses and to receive from it the requests of ancillary services. For V2G apparatuses of low power, it appears evident the convenience that a number of them operate in an aggregate way so as to be seen by the grid as a single apparatus of reasonable power.

Typical energy sources of a smart-grid are renewable sources (wind turbines, photovoltaic fields, mini-hydro). Each of them has specific operational features which influence the strategies of utilization of the sources, the design of the power converter interfacing the sources with the smart-grid, and the control of the sources. Due to the non-programmable energy generation of most of the renewable sources, the smart-grids are expected to include energy buffers. This functionality can be easily played by the batteries of the PEVs and, furthermore, is done on a distributed basis because of the location of PEVs over the country [10]-[11].

In order to study the integration between electric mobility and renewable energy sources, a micro-grid has been recently installed at the main campus of the University of Trieste [12]. It is composed of a 3.9 kWp photovoltaic generator, a 10 kWh storage battery interfaced to the micro-grid trough a 4.6 kVA inverter, a unidirectional charging station for electric cars with two 22 kW charging terminals and an interface board connecting the micro-grid to the 400 V university grid. An under-construction prototypal V2G apparatus is going to be added to the micro-grid, with the purpose of enhancing the potentialities of the micro-grid and enlarging the research topic.

In this paper, the prototypal V2G apparatus is described and its preliminary simulation tests are reported. In details, the rest of the paper is organized as follows. Section II describes the structure of the experimental V2G apparatus, including some sizing data, and justifies the most important design choices. Section III describes the control system with its low level units and high level unit. Section IV shows simulation results and Section V concludes the paper.

II. Experimental V2G apparatus

As mentioned above, a low-scale V2G experimental apparatus was designed and is under construction at the University of Trieste.

Many different structures of a V2G power electronics apparatus can be found in the literature [13]. As regards the connection of the V2G apparatus to the AC grid, the most immediate choice was to use a three-phase Voltage-Source Converter (VSC). On the other hand, the choice of the

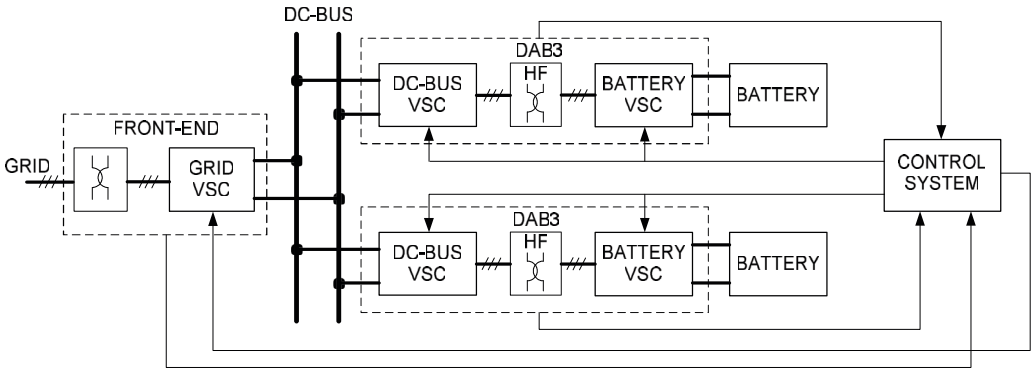

Fig. 1. Block scheme of the experimental V2G apparatus.

bidirectional DC/DC converter connecting the battery of the vehicle to the DC-side of the grid-connected VSC required the evaluation of a certain number of different possible structures [13]. Among them, we chose the most diffused in the literature, i.e. the dual-active bridge (DAB) [14]-[15], thanks to its high power density symmetrical structure and the possibility to include a high frequency isolation transformer. Anyway, actually the final choice fell on the isolated three-phase dual-active bridge (DAB3), composed of two three-phase VSCs and a three-phase high frequency transformer [16]. The choice of the DAB3 in place of the more diffused DAB, is due to the additional advantage of being composed of two bridges which have one more leg, offering a greater average current sharing, suitable mainly for the battery-connected VSC, and giving the possibility of providing fault tolerant operation in case of a faulty leg. Even if fault tolerance may appear to be not essential for battery charges, nevertheless it is an important feature helping to increase energy availability for electric cars and therefore to reduce the so called "range anxiety", which is one of the major obstacles to diffusion of EVs. Moreover, in V2G systems, it increases the reliability of ancillary services offered to the electric network.

Usually, in a charging station more than one vehicle can be connected to charge its battery. Consequently, the V2G apparatus, schematized in Fig. 1, was designed to be connected to two 3.3 kWh 52 V lithium-ion polymer (LiPo) batteries, each one connected to the 750 V DC-bus of the V2G apparatus via a DAB3 DC/DC converter. The battery three-phase VSC of the DAB3 is sized to be able to charge the 63 Ah battery at a rate of about 2C and to draw from it the same current, i.e. 130 A.

The V2G apparatus is completed by a grid VSC with the DC side connected to the 750 V DC-bus, endowed with a 4 mF capacitor C, and the AC side connected to the 400 V university grid via 2 mH filtering inductances L_f and an isolation transformer. By a modification of the transformer connections, the three-phase VSC has also the possibility to work in single-phase mode. In an advance experimental stage, when the V2G apparatus and its control system will have been extensively tested, the grid VSC can be directly connected to the university power system, excluding the isolation transformer.

III. Control System

The control system of the V2G apparatus is based on a dSpace [17] platform endowed with FPGA boards allowing fast dynamic control. The control algorithm is divided into four different units, namely the DAB3 control unit, the front-end control unit, the DC-bus control unit and the V2G control unit, i.e. a higher level control unit controlling the whole V2G apparatus.

A. DAB3 control unit

The control system of the V2G apparatus includes two DAB3 control units, one for each DAB3. The DAB3 control unit is devoted to the control of the power flowing through the DAB3 in order to transfer energy from the DC-bus to the battery and vice versa.

The two VSCs composing the DAB3 are controlled with a switching frequency of 20 kHz in order to obtain a 50% duty cycle square wave at their AC side. As explained in [16], the average power flowing through the DAB3 is a function of the displacement angle ϕ between the two square waves produced by each VSC and applied at the primary and secondary winding of the high-frequency transformer connecting the two VSCs.

The schematic of the DAB3 control unit captured from the graphical interface of the simulation platform PLECS [18] is shown in Fig. 2.

The DAB3 control unit receives as an input the reference power $P_{ref,DAB}$ to be absorbed or to be delivered by the DAB3. By $P_{ref,DAB}$, the angle ϕ_{ff} is calculated using the inverse of the equation, found in [16], giving the average transmitted power P_t for ϕ in the range (-π/3, π/3), i.e.

$$\phi = f(P_t) = \frac{2}{3}\pi\left(1 - \sqrt{1 - \frac{9\omega L P_t}{2\pi D V_1^2}}\right) \quad (1)$$

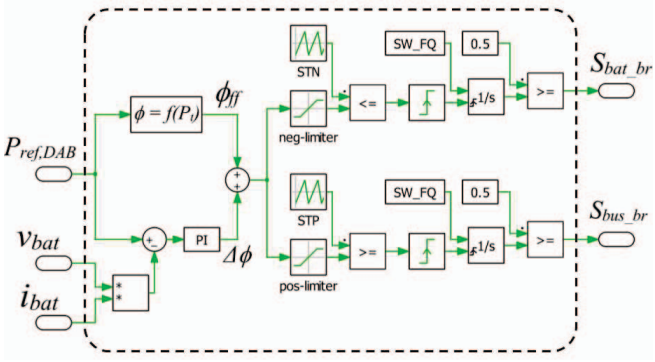

Fig. 2. PLECS block scheme of the DAB3 control unit.

In order to obtain a robust and precise power control, a closed loop control is added to the feedforward control. Angle ϕ is therefore obtained by adding ϕ_{ff} to an angle $\Delta\phi$ given by a PI controller processing the error between $P_{ref,DAB}$ and P_t, being P_t calculated as the product between the measured battery current i_{bat} and the measured battery voltage v_{bat}. Parameters of the PI controller are calculated in order to obtain a control bandwidth of 1.5 kHz when ϕ is equal to its maximum value $\pi/3$. Since the function $f(P_t)$ linking ϕ to P_t is not linear, the bandwidth changes with ϕ. Actually, when ϕ decreases the bandwidth increases. The maximum increase is reached when $\phi = 0$ and is equal to one third. As a consequence, the control loop bandwidth varies from 2 kHz to 1.5 kHz for ϕ varying from zero to $\pi/3$.

Angle ϕ is limited between zero and $-\pi/3$ by the neg-limiter and between zero and $\pi/3$ by the pos-limiter. Outputs of the limiters are respectively ϕ_{neg} and ϕ_{pos}.

Angle ϕ_{neg} is compared to the negative sawtooth wave STN of peak value -2π. When STN becomes lower than ϕ_{neg}, the output of the comparator switches to one and triggers the positive edge detector which outputs a pulse resetting the integrator 1/s. The input of the integrator is the switching frequency, so that during a switching period its output varies from zero to one. Finally, the output of the integrator is compared to 0.5 in order to produce a square wave signal S_{bat_br} with 50% duty cycle, driving the battery VSC.

On the other hand, ϕ_{pos} is compared to the positive sawtooth wave STP of peak value 2π. A square wave signal S_{bus_br} of 50% duty cycle is then produced in the same way as the previous one. It drives the DC-bus VSC.

When the battery has to be charged $P_{ref,DAB}$ is negative, thus causing ϕ_{neg} to be negative and ϕ_{pos} to be zero. In this way the square wave produced by the battery VSC is delayed by ϕ from the one produced by the DC-bus VSC and the energy flows from the DC-bus to the battery. When the battery has to deliver power, $P_{ref,DAB}$ is positive, thus causing ϕ_{neg} to be zero and ϕ_{pos} to be positive. In this way the square wave produced by the DC-bus VSC is delayed by ϕ from the one produced by the battery VSC and the energy flows from the battery to the DC-bus.

B. Front-end control unit

The front-end control unit is devoted to the control of the grid VSC. Its PLECS schematic is shown in Fig. 3.

The front-end control unit receives as an input the reference instantaneous real power p_{ref} and reference instantaneous imaginary power q_{ref} (defined by the p-q theory [19]) to be exchanged with the electric grid according to the active sign convention. Given p_{ref}, q_{ref} and the measured grid voltages v_{sa}, v_{sb}, v_{sc}, transformed to $v_{s\alpha}$, $v_{s\beta}$ according to the amplitude invariant abc-αβ transformation, the reference currents $i_{\alpha,ref}$, $i_{\beta,ref}$ of the grid VSC are then calculated as follows [19]

$$i_{\alpha,ref} = \frac{v_{s\alpha}\cdot p_{ref} + v_{s\beta}\cdot q_{ref}}{v_{s\alpha}^2 + v_{s\beta}^2}$$
$$i_{\beta,ref} = \frac{v_{s\beta}\cdot p_{ref} - v_{s\alpha}\cdot q_{ref}}{v_{s\alpha}^2 + v_{s\beta}^2} \quad (2)$$

The measured currents i_a, i_b, i_c, transformed to i_α, i_β according to the amplitude invariant abc-αβ transformation,

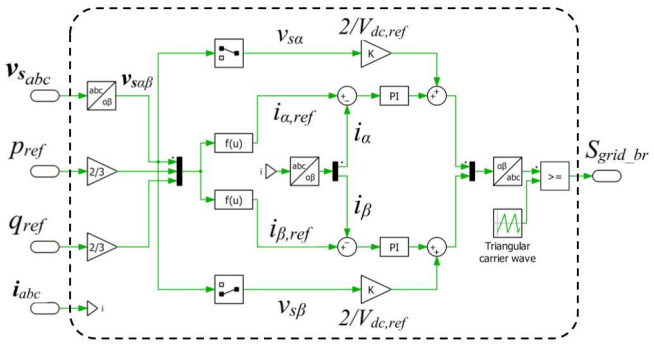

Fig. 3. PLECS block scheme of the front-end control unit.

are then subtracted to $i_{\alpha,ref}$, $i_{\beta,ref}$ and the errors are processed by two PI controllers outputting the voltage drops across L_f. The outputs of the PI controllers are added to $v_{s\alpha}$, $v_{s\beta}$ divided by half the DC-bus voltage V_{dc} in order to obtain $v_{FE\alpha,ref}$, $v_{FE\beta,ref}$, i.e. the p.u. reference values of the grid VSC output voltage in the αβ reference frame. Finally, $v_{FE\alpha,ref}$, $v_{FE\beta,ref}$ are submitted to the inverse amplitude invariant abc-αβ transformation, obtaining the modulating signals for the sub-oscillation PWM producing the 20 kHz driving signals S_{grid_br} for the grid VSC.

Parameters of the PI controllers are calculated in order to obtain a control loop bandwidth of 2 kHz.

If the non-optimal quality of the grid voltage or dynamic demanding services such as harmonic filtering require higher performance current control, the PI-based control loops can be substituted with more sophisticated current control systems such as the ones developed in [20].

C. DC-bus control unit

The DC-bus control unit is devoted to the control of V_{dc}, assuring the balance between losses, power exchanged by the DAB3s and power exchanged by the front-end. It is based on the following power balance s-domain linear equation:

$$s\frac{C}{2}V_{dc}^2 = P_{DAB1} + P_{DAB2} - 3V_s I_a \quad (3)$$

where P_{DAB1}, P_{DAB2}, V_s, I_a are respectively the output powers of the two DAB3s, the rms value of the grid voltage and the rms value of the grid VSC output current component in phase with the grid voltage. By (3) the controlled variable is V_{dc}^2, as it is shown by the PLECS schematic of Fig. 4, where the squared value of the measured V_{dc} is subtracted to the squared value of its reference $V_{dc,ref}$. The error is then processed by a PI controller in order to obtain the instantaneous real power p_{loss} needed to restore the losses and assure the power balance inside the V2G apparatus. Parameters of the PI controller are calculated in order to obtain a loop bandwidth of 200 Hz.

The output p_{loss} of the DC-bus control unit is sent to the V2G control unit.

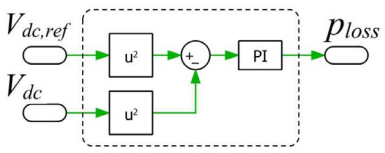

Fig.4. PLECS block scheme of the DC-bus control unit.

D. V2G control unit

The V2G control unit includes a high level control algorithm coordinating the control units described above and controlling the charge and discharge of the batteries according to a strategy conciliating the charging needs with the requested ancillary services requiring an exchange of active power. Moreover, it has to exchange information with the grid, receiving the requests of ancillary services and giving feedbacks about the actual possibility to provide them.

The PLECS schematic of the implemented V2G control unit is shown in Fig. 5. It receives the following inputs: the request of active power P_{req} and reactive power Q_{req} to be delivered to the grid, the charging commands CHG_1 and CHG_2 for the batteries (set to 0 for charge not required and 1 for charge required), the SOCs and voltages of the two batteries and p_{loss}.

The algorithm of the V2G control unit operates as explained in the following. If both CHG_1 and CHG_2 are set to 0, then the V2G apparatus can satisfy the request P_{req} within the limits of its capability and according to a strategy based on SOC of batteries, as described in the following.

1) P_{req} is positive, i.e. the V2G apparatus is requested to deliver active power to the grid. a) If both batteries have SOC ≥ 10% then $P_{ref,DAB}$ is set equal to $(P_{req} + p_{loss})/2$ and sent to both DAB3 control units. The reference p_{ref} for the grid VSC is set equal to P_{req}. b) If one of the two batteries has SOC < 10% $P_{ref,DAB}$ is set to zero for its DAB3 while $P_{ref,DAB}$ is set equal to $(P_{req} + p_{loss})$ for the other DAB3, which will deliver it or, if it is higher than its capability, the maximum possible. Again, p_{ref} is set equal to P_{req} or to the actual power delivered by the DAB3. c) If both batteries have SOC < 10%, then $P_{ref,DAB}$ is set to zero for both DAB3s and p_{ref} is set equal to $-p_{loss}$.

2) P_{req} is negative, i.e. the V2G apparatus is requested to absorb active power to be stored in the batteries. a) If both batteries have SOC ≤ 90% then $P_{ref,DAB}$ is set equal to $P_{req}/2$ and sent to both DAB3 control units. The reference p_{ref} for the grid VSC is set equal to $P_{req} - p_{loss}$. b) If one of the two batteries has 90% < SOC < 100%, then power absorbed by the corresponding DAB3 is halved and the other DAB3 absorbs the rest of P_{req} or the maximum allowed by its capability. Again, p_{ref} is set equal to $P_{req} - p_{loss}$ or to the actual total power absorbed by the two DAB3. c) If one of the two batteries has SOC = 100%, then power absorbed by the corresponding DAB3 is zeroed and the other DAB3 absorbs all P_{req} or the maximum allowed by its capability. Once again, p_{ref} is set equal to $P_{req} - p_{loss}$ or to the actual power absorbed by the working DAB3. d) If both batteries have SOC = 100%, then $P_{ref,DAB}$ is set to zero for both DAB3s. In this case p_{ref} is set equal to $-p_{loss}$, so that the V2G apparatus absorbs only its losses from the grid, thus not being able to satisfy the request to store energy in the batteries.

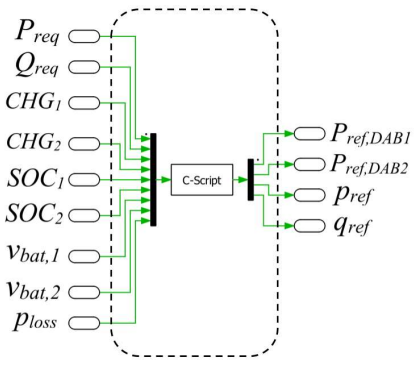

Fig.5. PLECS block scheme of the V2G control unit.

The request of battery charging has priority over any other request. Therefore, if CHG_1 or CHG_2 is set to 1 the corresponding $P_{ref,DAB}$ is negative and calculated in order to charge the battery at 130 A up to SOC = 90% and then current is halved until the SOC reaches 100%. The other DAB3, depending on the SOC of its battery and the value and sign of P_{req}, can totally, partially or cannot satisfy the power request. For instance, if P_{req} is negative the request can be satisfied up to the V2G apparatus capability. On the contrary, if P_{req} is positive the request cannot be satisfied, but the power absorbed from the grid can be zeroed or at least reduced transferring energy from one battery to the other.

Finally, if both CHG_1 and CHG_2 are set to 1, $P_{ref,DAB}$ is negative, calculated in order to charge the batteries at 130A and sent to both DAB3 control units. In this case delivery of P_{req} is inhibited and p_{ref} is set equal to $(2P_{ref,DAB} - p_{loss})$, i.e. the grid VSC has to absorb from the grid $2P_{ref,DAB}$ plus the losses.

IV. Simulation Results

The described prototypal V2G apparatus and its control system has been modeled in the PLECS simulation environment. Its schematic, captured from the PLECS graphical interface, is shown in Fig. 6 and includes both the circuitry and the control system. The circuitry is composed of two batteries (modeled with the equivalent circuit and equations found in [21]), two DAB3s (composed of the battery VSC, the high-frequency transformer and the DC-bus VSC), the DC-bus with its capacitor, the grid VSC with its filtering inductances and the power system. The control system is composed of two DAB3 control units ($DAB3_1$ CU and $DAB3_2$ CU), the front-end control unit (FE CU), the DC-bus control unit (DC-bus CU) and the high level control unit, i.e. V2G control unit (V2G CU).

The V2G apparatus has been submitted to a number of tests to check the good operation of the system also in the most demanding transient conditions, where reference power variations are limited by a rate limiter of 2.5 kW/ms. The most significant quantities useful to evaluate the operation of the system are the DC-bus voltage V_{dc}, the battery currents i_{bat1}, i_{bat2} and the AC output currents of the grid VSC i_a, i_b, i_c. The results of three tests, where the starting SOC of both batteries is set to 50%, are described in the following.

In the first test, both the charging signals CHG_1 and CHG_2 are zero and the V2G apparatus is supplying the grid with a reactive power Q_{req} = 4 kVAR and an active power P_{req} = 4 kW, being the last one supplied half by $DAB3_1$ and half by $DAB3_2$. Also the losses are supplied half by $DAB3_1$ and half by $DAB3_2$. Traces of the quantities listed above are displayed in Fig. 7, showing the good operation of the apparatus in steady state condition and also during a transient, after that, at time t_1 = 0.2 s, CHG_1 is switched to 1. At this event, the V2G control unit commands: a) $DAB3_1$ to stop delivering power and start absorbing power in order to charge the battery, b) $DAB3_2$ to deliver all P_{req} plus all the losses, c) the grid VSC to continue to deliver Q_{req} and to absorb the rest of the power needed to charge the battery at the desired current of 130 A.

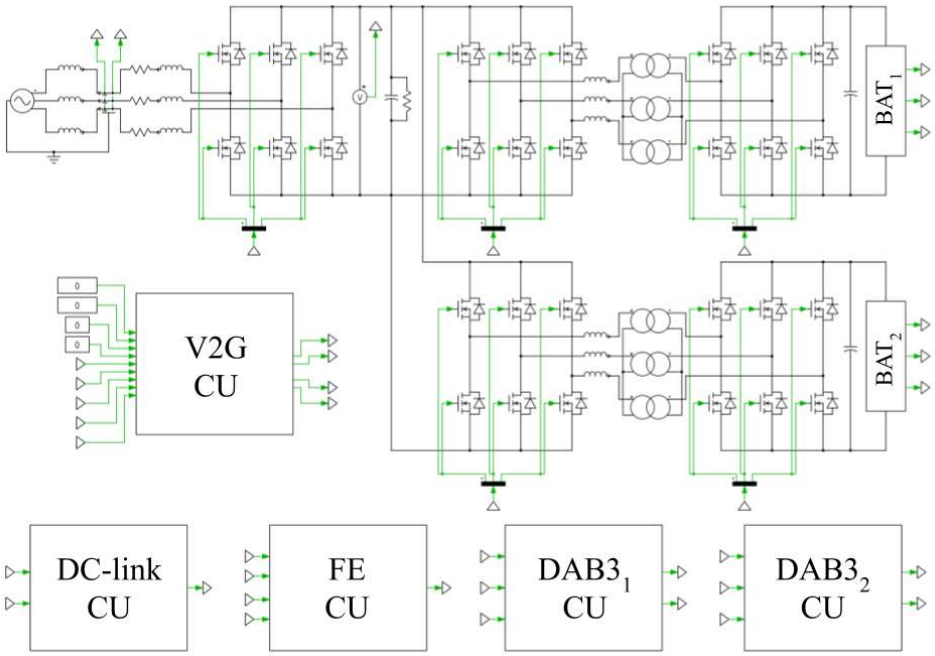

Fig.6. PLECS schematic of the V2G apparatus and its control system.

Fig. 7 shows that transient of battery currents and AC output currents last a few milliseconds, while transient of V_{dc} lasts almost 50 ms, but the amplitude fluctuation is negligible.

A different possible strategy could be the one to command the $DAB3_2$ to deliver the maximum power allowed by its capability. In this way, battery 1 would be charged only with the energy of battery 2 and the active power absorbed from the grid would be zeroed.

In the second test, the ability of the V2G apparatus to face the wide power variations required by the most demanding grid requests is checked. Both CHG_1 and CHG_2 are zero during the whole test. At the beginning the V2G apparatus is supplying the grid with Q_{req} = 9 kVAR and P_{req} = 12 kW, being the last one supplied half by $DAB3_1$ and half by $DAB3_2$. At time t_1 = 0.2 s, the grid request is suddenly changed to P_{req} = –12 kW, i.e. the V2G apparatus is requested to absorb power in order to store excess available energy in the batteries. The V2G control unit commands: a) $DAB3_1$ and $DAB3_2$ to stop delivering power and start absorbing $P_{req}/2$ each, b) the grid VSC to continue to deliver Q_{req} and to absorb P_{req} plus the losses from the grid. Test results are displayed in Fig. 8, where it is shown that transient of battery currents and AC output currents last roughly 10 ms, while transient of V_{dc} lasts almost 60 ms. In this case the amplitude fluctuation of V_{dc} is not negligible, but it is definitely acceptable, being limited to about 3%.

In the third test, at the beginning both CHG_1 and CHG_2 are zero and the V2G apparatus is supplying the grid with Q_{req} =

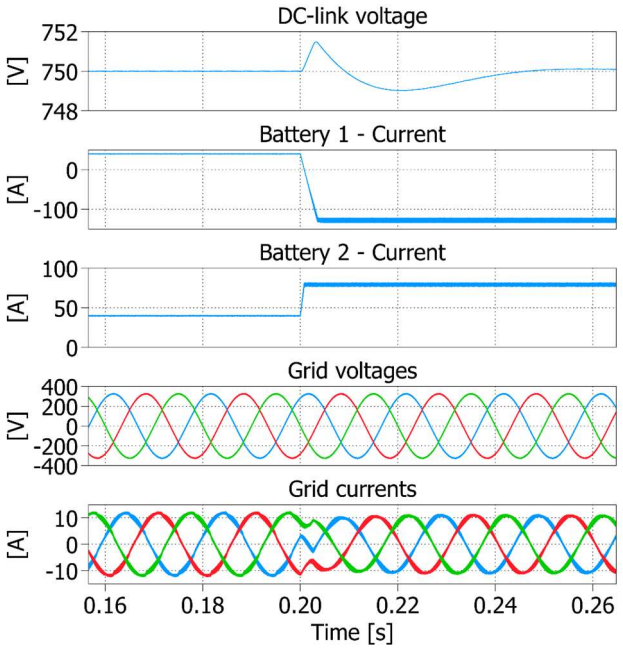

Fig.7. Test 1: DC-bus voltage, battery currents, grid voltages and output currents of the grid VSC.

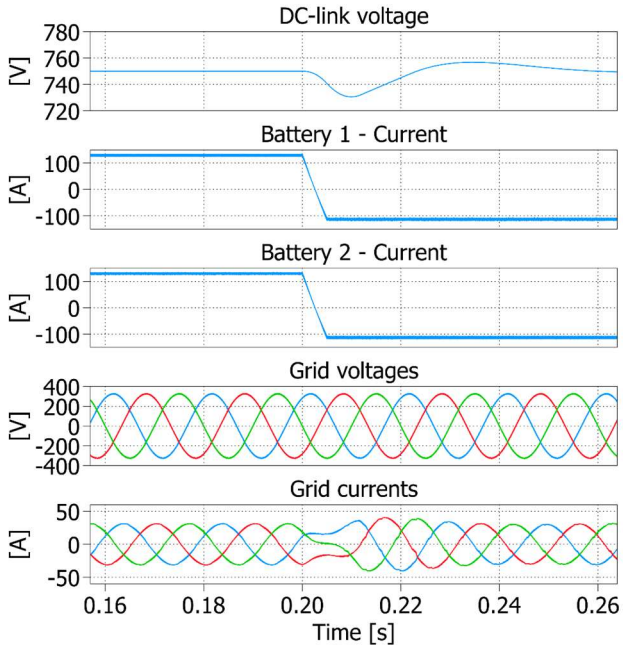

Fig.8. Test 2: DC-bus voltage, battery currents, grid voltages and output currents of the grid VSC.

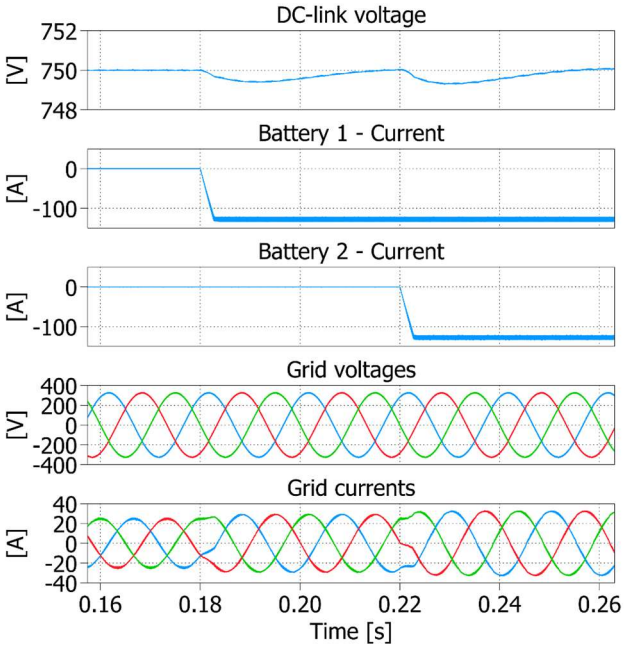

Fig.9. Test 3: DC-bus voltage, battery currents, grid voltages and output currents of the grid VSC.

12 kVAR, while it absorbs from the grid only the losses, because $P_{req} = 0$. At time $t_1 = 0.18$ s, CHG_1 is switched to 1 and the V2G control unit commands: a) $DAB3_1$ to start absorbing power in order to charge the battery at 130 A, b) $DAB3_2$ to stay in standby, c) the grid VSC to continue to deliver Q_{req} and to absorb the power needed to charge the battery plus the losses. As mentioned in the explanation of the first test, a different possible strategy is to take the energy to charge battery 1 from battery 2. At time $t_2 = 0.22$ s, also CHG_2 is switched to 1 and the V2G control unit commands: a) both $DAB3_1$ and $DAB3_2$ to absorb power in order to charge the batteries at 130 A, b) the grid VSC to absorb the power needed to charge the batteries plus the losses and to reduce to 6 kVAR the delivered reactive power in order not to exceed its capability. Of course, in this case the reactive power request is only partially satisfied. Fig. 9 shows the test results highlighting once again the good performance of the V2G apparatus, proved by the very fast transients of battery currents and AC output currents and completely negligible fluctuations of V_{dc}.

V. Conclusions

In this paper, a prototypal V2G apparatus under construction is presented. The apparatus is described, modeled in the PLECS environment and preliminarily tested by simulations. The different control units composing the control system are described in detail. Results of three tests are shown and commented. They prove the good operation of the V2G apparatus and its excellent performance.

Upcoming developments concern the experimental test of the grid VSC, which has just become available, and the further development of the V2G control unit with more sophisticated control strategies and the addition of the possibility to compensate the reactive power and the current harmonics absorbed by specific loads, i.e. to perform the power line conditioning service.

References

[1] C. Liu, K. T. Chau, D. Wu, and S. Gao, "Opportunities and challenges of vehicle-to-home, vehicle-to-vehicle, and vehicle-to-grid technologies", *Proc. of the IEEE*, Vol.101, No. 11, pp. 2409-2427, Nov. 2013.

[2] M. Yilmaz, and P. T. Krein, "Review of the impact of vehicle-to-grid technologies on distribution systems and utility interfaces", *IEEE Trans. on Power Electronics*, Vol. 28, No. 12, pp. 5673-5689, Dec. 2013.

[3] N. Z. Xu and C. Y. Chung, "Reliability evaluation of distribution systems including vehicle-to-home and vehicle-to-grid", *IEEE Trans. on Power Systems*, Vol. 31, No. 1, pp. 759-768, Jan. 2016.

[4] Y. Zheng, S. Niu, Y. Shang, Z. Shao, and L. Jian, "Integrating plug-in electric vehicles into power grids: A comprehensive review on power interaction mode, scheduling methodology and mathematical foundation", *Renewable and Sustainable Energy Reviews*, Vol. 112, pp. 424-439, Sept. 2019.

[5] G. Buja, M. Bertoluzzo, and C. Fontana, "Reactive power compensation capabilities of V2G-enabled electric vehicles", *IEEE Trans. on Power Electronics*, Vol. 32, No. 12, pp. 9447-9459, Dec. 2017.

[6] M. Brenna, F. Foiadelli, and M. Longo, "The exploitation of vehicle-to-grid function for power quality improvement in a smart grid", *IEEE Trans. on Intelligent Transportation Systems*, Vol. 15, No. 5, pp. 2169-2177, Oct. 2014.

[7] K. M.Tan, V. K.Ramachandaramurthy, and J. Y. Yong, "Integration of electric vehicles in smart grid: a review on vehicle to grid technologies and optimization techniques", *Renewable and Sustainable Energy Reviews*, Vol. 53, pp. 720-732, Jan. 2016.

[8] H. S. V. S. K. Nunna, S. Battula, S. Doolla, and D. Srinivasan, "Energy management in smart distribution systems with vehicle-to-grid integrated microgrids", *IEEE Trans. on Smart Grid*, Vol. 9, No. 5, pp. 4004-4016, Sept. 2018.

[9] V. Monteiro, J.G. Pinto, and J. L. Afonso, "Improved vehicle-for-grid (iV4G) mode: Novel operation mode for EVs battery chargers in smart grids", *Int. Journal of Electrical Power and Energy Systems*", Vol. 110, pp. 579-587, Sept. 2019.

[10] M. J. E. Alam, K. M. Muttaqi, and D. Sutanto, "Effective utilization of available PEV battery capacity for mitigation of solar PV impact and grid support with integrated V2G functionality", *IEEE Trans. on Smart Grid*, Vol. 7, No. 3, pp. 1562-1571, May 2016.

[11] H. Mehrjerdi, and E. Rakhshani, "Vehicle-to-grid technology for cost reduction and uncertainty management integrated with solar power", *Journal of Cleaner Production*, Vol. 229, pp. 463-469, Aug. 2019.

[12] A. Massi Pavan, V. Lughi, and M. Scorrano, "Total cost of ownership of electric vehicles using energy from a renewable-based microgrid", in proc. of IEEE PowerTech, pp. 1-6, Milan, 2019.

[13] A. Sharma, S. Sharma, "Review of power electronics in vehicle-to-grid systems", *Journal of Energy Storage*, Vol. 21, pp. 337-361, Feb. 2019.

[14] S. Inoue, and H. Akagi, "A bidirectional DC–DC converter for an energy storage system with galvanic isolation", *IEEE Trans. on Power Electronics*, Vol. 22, No. 6, pp. 2299-2306, Nov. 2007.

[15] C. Mi, H. Bai, C. Wang, and S. Gargies, "Operation, design and control of dual H-bridge-based isolated bidirectional DC–DC converter", *IET Power Electronics,* Vol. 1, No. 4, pp. 507-517, Dec. 2008.

[16] R.W.A.A. De Doncker, D.M. Divan, and M.H. Kheraluwala, "A three-phase soft-switched high-power-density dc /dc converter for high-power applications", *IEEE Trans. on Industry Applications*, Vol. 27, No. 1, pp. 63-73, Jan./Feb. 1991.

[17] dSPACE GmbH, https://www.dspace.com/en/pub/home.cfm.

[18] Plexim GmbH, "PLECS User Manual", available for download at https://plexim.com/sites/default/files/plecsmanual.pdf.

[19] H. Akagi, E.H. Watanabe, and M. Aredes, *Instantaneous power theory and applications to power conditioning*, Chapter 3, John Wiley and Sons, Inc., Wiley-IEEE Press; 2007.

[20] S. Castellan, G. Buja, and R. Menis, "Single-phase power line conditioning with unity power factor under distorted utility voltage", *Int. Journal of Electrical Power and Energy Systems*, Vol. 121, pp. 1-10, October 2020.

[21] G. L. Plett, *Battery management systems – Volume 1: battery modeling*, Artech House, 2015.